JOURNAL OF MAGNETIC RESONANCE **126,** 207–212 (1997)
ARTICLE NO. MN971174

Stray-Field Imaging of Planar Films Using a Novel Surface Coil

P. M. Glover, P. J. McDonald, and B. Newling

Department of Physics, University of Surrey, Guildford, Surrey GU2 5XH, United Kingdom

Received October 25, 1996; revised March 24, 1997

A surface-coil approach to stray-field magnetic resonance imaging (STRAFI), which has certain advantages for the profiling of planar films and layers, is described. Frequency-swept and Fourier-transform versions of the experiment, which are particularly suitable for use with the coil, are reported. As an example application, a latex coating is analyzed during the evaporative drying process, in which a colloidal dispersion is transformed to a continuous polymer film. The ultimate achievable resolution is discussed and contrasted with conventional MR microscopy.

INTRODUCTION

Stray-field imaging (STRAFI) (*1*) has created a wide range of opportunities for the imaging of solids and other samples having a short T_2 (<100 μs). Many of these are of interest to materials scientists for industrial applications. The STRAFI technique exploits the large fringe field gradient surrounding high-field magnets. Near the base of a typical 9.4 T 89 mm vertical-bore magnet, the static-field strength equates to a proton resonant frequency of 235 MHz, superimposed on a static gradient of 58 T m^{-1}. Typically in conventional STRAFI a short, hard 10 μs pulse is used to excite resonance in a thin slice of the sample of thickness on the order of 40 μm. The gradient is sufficient to ensure that the gradient-induced broadening over such a slice is greater than the most severe dipolar linewidth. Any local susceptibility line broadening in heterogeneous samples is also dominated by the applied gradient. Following excitation the magnetization is observed in the form of an echo following a second pulse and is recorded as a measure of the proton density within the slice. The sample is then mechanically translated along the axis of the static field and the measurement repeated so as to build up a profile of the sample in one dimension. For 3D images, the sample is rotated and the procedure repeated for a series of different projections (*2*). This procedure is time consuming and so dynamic studies are usually arranged and carried out in one dimension only (*3*).

The disadvantage of the stray-field profiling technique is that only samples that are invariant in the x–y plane are suitable. In most cases, invariance can be arranged with precise leveling and careful sample preparation. Leveling is difficult but may be achieved either mechanically (*4*) or, in principle, with electrical shim gradient coils. However, in some instances, it is not possible to arrange for the experiment to be one dimensional. An example is the drying of layers of colloidal dispersions, such as sols and emulsions. Here the meniscus of the sample leads to a rounded surface and surface shrinkage leads to wrinkling, both of which compromise profiling through the whole sample. Another example is the study of liquid ingress into solids where ingress into the sides of the sample can be limiting.

The objective of this paper is, therefore, to introduce an MRI method of studying systems which start mobile and end up with short to medium T_2 components (or vice versa), which are thus inaccessible to conventional microscopy ($T_2 \leqslant 1$ ms) and which cannot easily be arranged in one-dimensional forms. Examples include the drying of paint films as demonstrated in this paper, and also the ingress of solvents into polymer systems where the response of the short T_2 polymer is of interest (*5*). In this paper, we propose a localization coil for use with STRAFI operating below a standard magnet. The coil selectively excites a small central region of a much larger sample. With STRAFI, this is the only way that a small area of the x–y sample plane, which approximates much better to a planar sample, can be localized. A second advantage of the coil is that because only a small region of a large sample is being studied, the problems associated with leveling the sample are substantially reduced by the lever principle. However, since the sample can no longer be moved independently of this coil, alternative profiling strategies to pulse-physical translation are introduced.

EXPERIMENTAL

A schematic diagram of the film coil is shown in Fig. 1. The coil axis is arranged along the x axis, perpendicular to the main magnetic field and the gradient axis, z. The geometry of this coil is novel because it uses the axial B_1 field component of a solenoid, outside the central volume. In most surface coil applications, the sample is placed at the end of the coil to maximize B_1 and hence the sensitivity. In our STRAFI system based on a standard vertical-bore magnet,

1090-7807/97 $25.00

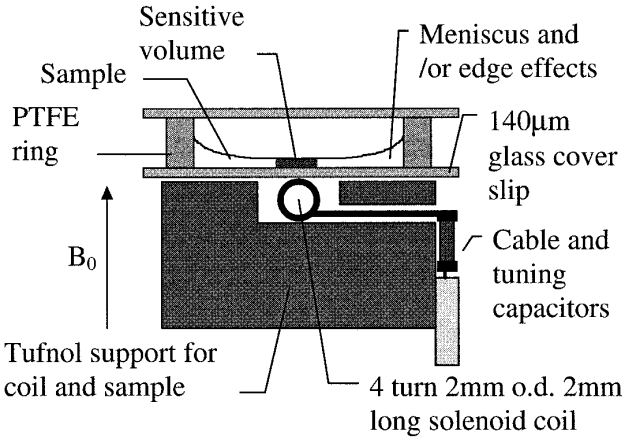

FIG. 1. A schematic of the RF coil used in this work viewed along the *x* axis and showing a suitable sample cell in the imaging position.

this arrangement is impossible because the useful gradient g_z is coaxial with the main field B_0. The B_1 field must be orthogonal to B_0 so therefore it is also orthogonal to g_z. The signal-to-noise ratio is severely compromised with respect to that which would be obtained from the same sample volume under more regular conditions, but this is accepted because only by this method can satisfactory profiles be obtained of the systems in question. A 22 mm diameter cylinder of Tufnol is used to support the coil and the sample cell. A four-turn, 2 mm diameter, 2 mm long solenoid is glued into a recess in the top of the support. The tune and match components are mounted on the side of the support and are connected to the spectrometer using copper-cored rigid coax cable. The bandwidth of the coil is 4.3 MHz giving a Q of 54, which makes it suitable for solids work. The glue, Tufnol, and solder flux proton signals are not detected by the imaging experiment as their resonant frequencies fall well out of the bandwidth of the experiment (58 T m^{-1} equates to 2.3 MHz mm^{-1} for protons). Figure 1 also shows a typical sample cell for use with the coil that is suitable for liquid ingress work. The assembly is mounted on the STRAFI imaging probe stage but without the mechanical stepper drive engaged.

The theoretical component of the B_1 field strength in the orthogonal plane to the static field for this coil, calculated using the Biot–Savart law and numerical integration around the current loops, is shown as contour plots in Fig. 2 where the origin of the coordinate system is taken as the coil center. The contours are at 1.5% intervals with 100% being the field at the center of the solenoid. The absolute figures indicate how much the signal-to-noise ratio has been compromised in order to achieve the necessary localization. Figure 2a shows the magnitude of the B_1 field in the z–x plane for $y = 0$, and Fig. 2b shows the x–y plane for $z = 1.4$ mm. This z position corresponds to the base of a sample placed on a glass cover slip. The ripples near the coil are due to the finite wire spacing. The plots show that the coil localizes to the order of the length of the coil along the x axis, and to the order of the diameter in the y direction. Plots as a function of z show that the area of similar sensitivity increases with distance from the coil; thus the sample volume effectively increases. This effect offsets the sensitivity reduction at a distance and partially flattens out the spatial response of the coil. It is also possible to adjust the pulse power as the sample is imaged to compensate for reduced tip angle at a distance. We have found that the usable field of view possible with this coil is nominally 800 μm deep. We have further found that it is useful to perform a calibration experiment using a thick rubber sample placed directly on top of the coil. The rubber profile may be used to normalize subsequent experiments. In the demonstrations described below, however, this calibration step has not been necessary, because the film thickness is significantly less than 800 μm.

The coil may be used with either a frequency-swept or a Fourier variant of STRAFI. Both methods have the considerable advantage over mechanically translated STRAFI in that the movement of the sample during the sequence does not cause measurement artifacts (*6*). Forms of the frequency-swept method were tried in the early days of stray-field imaging by various experimenters including Miller and Garroway (*7*), who dubbed the method planar imaging. In the frequency-swept variant introduced here, a standard, multiple, quadrature-echo pulse sequence α_x—τ—(α_y—τ—echo—τ)$_m$ is employed, where α_x is a nominal 90° pulse of relative phase x. The interpulse gap is denoted by τ, and m is the number of echoes. Just as in conventional STRAFI, the magnetization from different slices within the thin film is detected. The slice thickness is determined by the pulse length. The difference is that the NMR spectrometer frequency is incremented between slices rather than the sample position. This technique is fast, as there is no need to wait a T_1 recovery delay between slices or to move the sample. A frequency-interleaved sequence may also be implemented, minimizing any residual interslice overlap effects due to T_1. The lower trace of Fig. 3 shows a profile of two glycerol films sandwiched between glass cover slips and separated by a 100 μm thick acetate spacer. The average film thickness is estimated at 50 μm using gravimetric analysis. The pulse length used is 80 μs and the pulse gap, τ, is 100 μs. The frequency step size is 16 kHz, equivalent to 6.5 μm. Multiple echo train data have been recorded, and the profile shows eight echoes at each spatial location, albeit without high reproduction detail. This echo train may be analyzed to yield spatially localized relaxation information about the sample. A total of 256 averages were acquired in just under 5 min.

Fourier transform imaging in the fringe field is directly analogous to conventional microscopy (*8*) except that the gradient is static rather than dynamic. In the stray-field Fourier variant, the pulse length is made sufficiently small (on the order of 1 μs) so as to provide a bandwidth which

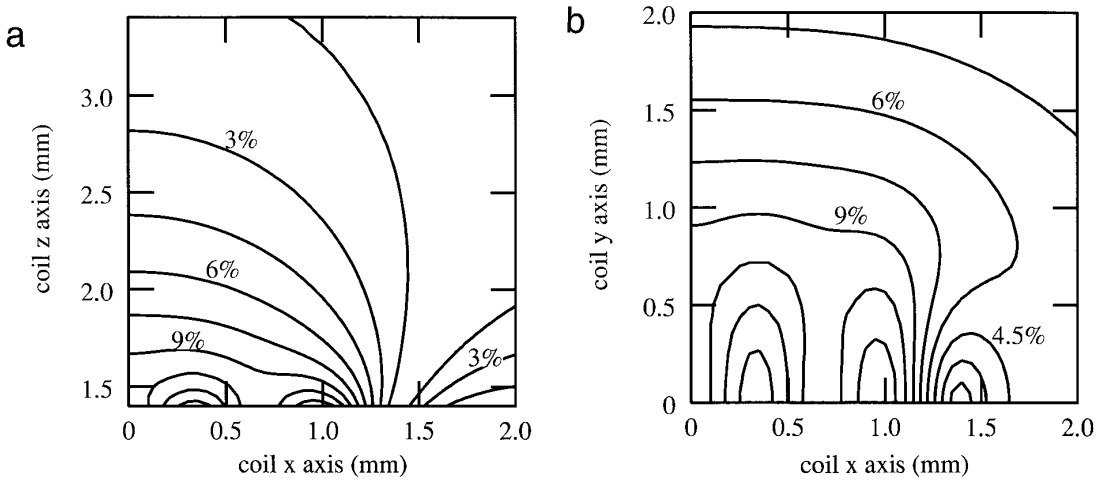

FIG. 2. Calculated contour plots of the coil B_1 magnetic field magnitude (a) in the vertical z–x plane for $y = 0$ mm, and (b) in the horizontal x–y plane for $z = 1.2$ mm.

spans the whole sample thickness, in this instance 400 μm (bandwidth on the order of 1 MHz). Samoilenko and Zick (*4*) have previously demonstrated stray-field Fourier imaging using a quadrature echo, with the sample enclosed by a very small coil. This approach is clearly inappropriate for thin films. We prefer to Fourier transform a standard spin echo to yield a one-dimensional profile. Since with our coil the pulse tip angle is a strong, rapidly decreasing function of depth into the film, we require a pulse sequence in which the echo formation is tip-angle insensitive and well suited to low-flip-angle pulses. A suitable sequence is $(\beta_x\text{—}\tau\text{—}2\beta_{-x}\text{—}\tau\text{—echo—TR})_n$ where β_x is a low-flip-angle pulse and n is the number of averages. This sequence is run under steady-state conditions with a short repetition time, TR, so that the small signal intensity consequent upon the small pulse is more than compensated by the rapid averaging that can be achieved (*9*). The upper trace in Fig. 3 shows the use of this sequence to image the same glycerol phantom as used in the frequency-swept experiment. The pulse length, t_p, is 0.5 μs ($\beta_x \approx 3°$ at the sample center) and τ is 125 μs. The delay TR was set to 1 ms, allowing 225,000 averages to be acquired in less than 4 min. The frequency-swept profile contains information about T_2 and diffusion in the echo train which is not seen in the Fourier profile. This could have been implemented in the Fourier method, however, with a multiple-echo sequence such as $[\beta_x\text{—}\tau\text{—}(2\beta_{-x}\text{—}\tau\text{—echo—}\tau\text{—}2\beta_x\text{—}\tau\text{—echo—}\tau)_m\text{—TR}]_n$.

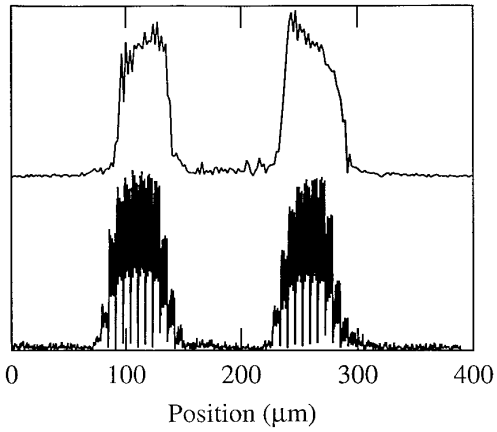

FIG. 3. Profiles of two 50 μm thick glycerol films sandwiched between glass cover slips and separated by a 100 μm thick acetate spacer acquired using frequency-swept (lower trace) and Fourier-transform spin-echo (upper trace) stray-field imaging.

We are currently using the coil and the methods described here as an ideal way to study the film formation of oil, oil-in-water emulsion, and latex paints, and for studies of solvent ingress into glassy polymers where the swollen phase typically has intermediate T_2. As a practical example, Fig. 4 shows the time course over a period of two hours of a water-based latex paint drying to a film on a glass cover slip. Initially, the coating consists of colloidal polymer particles dispersed in water. When drying is complete, a continuous polymer film is formed. The data were obtained using the frequency-swept technique with a frequency step equivalent to 20 μm. Profiles were obtained at 6 min intervals. The data were acquired in the form of 16 echo trains with a pulse gap, τ, of 18 μs (center to center) and a pulse length of 15 μs. The plots show profiles for the second, sixth, tenth, and fourteenth echoes. The first echo is not shown, as this is systematically of reduced intensity in STRAFI (*6*). The profiles clearly show water loss from the top surface of the film in the early stages of drying when water (long T_2) is the continuous phase. At longer times, there is a decrease in the signal intensity from the residual layer as more water is lost, and there is an associated dramatic shortening of T_2. We

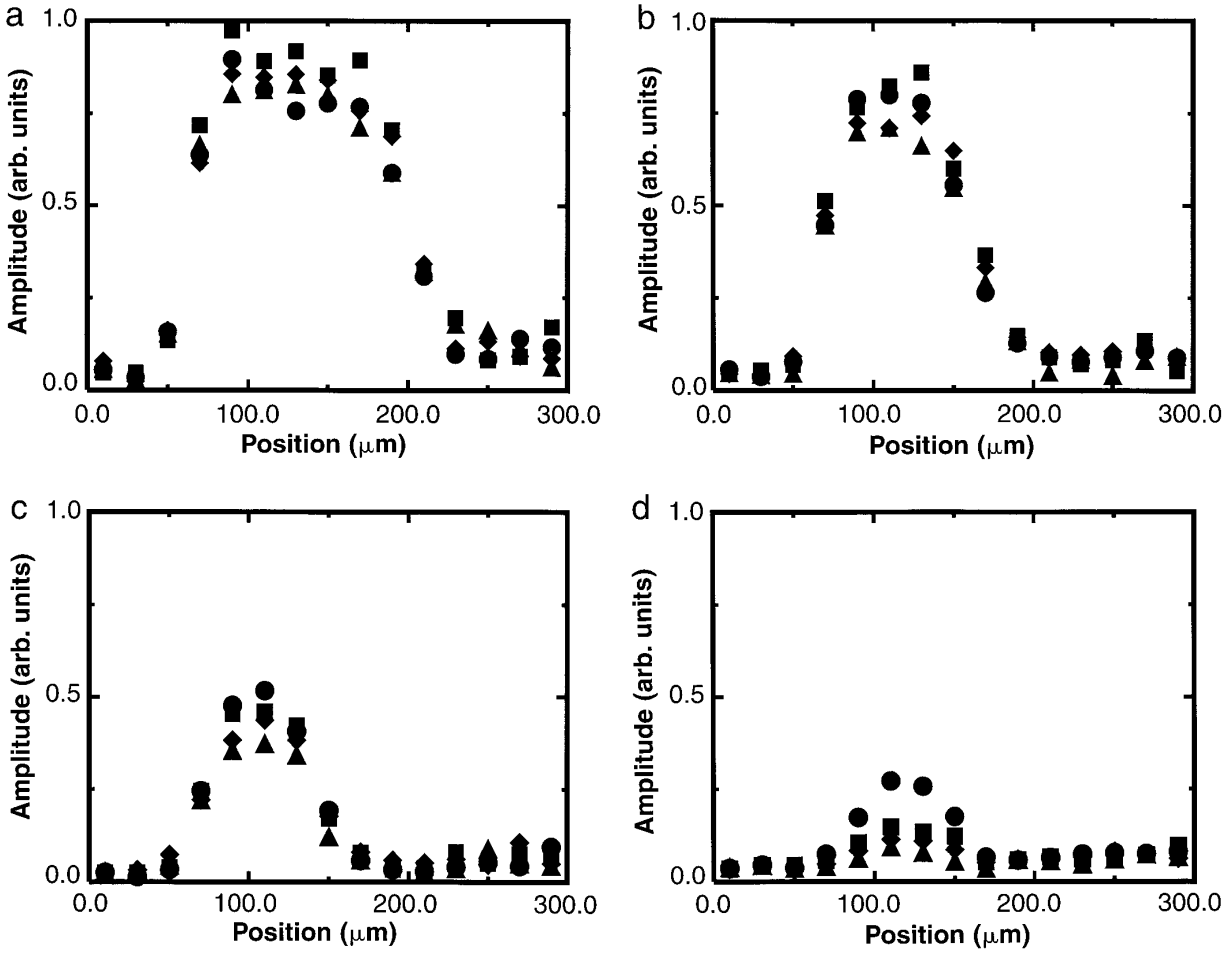

FIG. 4. Profiles recorded from a drying latex paint film recorded (a) immediately after coating the glass substrate, and then after (b) 24 min, (c) 36 min, and (d) 2 h. In each case, the 2nd (circles), 6th (squares), 10th (diamonds), and 14th (triangles) echo profiles are shown. The exposed surface is to the right.

observed no substantial changes in the measured profiles in the subsequent 12 h period. The T_2 of the dry latex paint has been separately measured, both in the fringe field as a film using a 90°_x—τ—180°_y—τ—echo pulse sequence with the echo recorded for different τ, and also from a dry bulk sample using a free-induction decay in a bench-top spectrometer operating at 20 MHz. In both cases, the measurement gave $T_2 = 55 \pm 5$ μs. In the profiles, the application of the quadrature-echo sequence causes partial spin locking, and there is evidence that the magnetization is being sustained in the profile echo trains due to $T_{1\rho}$ processes. The effective T_2 relaxation time of the nominally dry sample at 2 h, measured at the center of the film using the profile data, is 350 ± 15 μs.

DISCUSSION

For the glycerol demonstration profiles presented here, the pixel size for the Fourier method is 2 μm, three times smaller than for the frequency-swept method, and it could potentially reach 1 μm. It is instructive therefore to compare the theoretical image resolution obtainable using the two techniques, and indeed to compare both with conventional magnetic resonance microscopy. The slice thickness and hence pixel size, Δr, in conventional stray-field imaging and frequency-swept stray-field imaging is proportional to the inverse pulse length, t_p^{-1}, according to (*6*)

$$\Delta r = \frac{\sqrt{3}\pi}{\gamma g t_p}, \qquad [1]$$

where γ is the magnetogyric ratio and g the gradient strength. The longer the pulse, the better the resolution. However, the pulse length can be no longer than the pulse gap, τ, which, under optimal resolution conditions, is of order T_2, the spin–spin relaxation time. Hence,

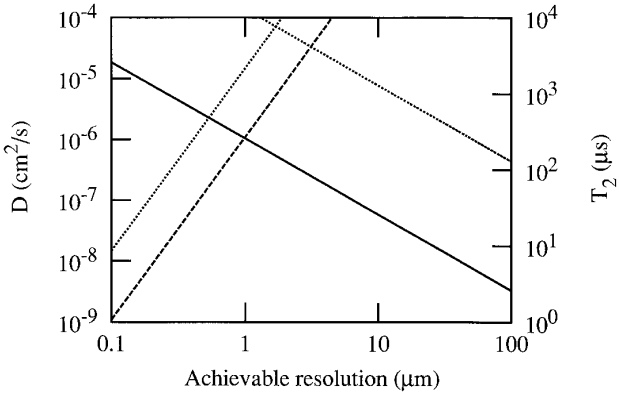

FIG. 5. The solid line shows the relationship between sample T_2 (right-hand axis) and best resolution using stray-field imaging. The dashed line shows the corresponding diffusion limit (left-hand axis) to the resolution in mobile systems. In both cases, it is assumed that the gradient strength, g, is 58 T m^{-1}. The parallel dotted lines show the corresponding values for a conventional microscopy experiment with $g = 1$ T m^{-1}.

$$\Delta r_{\text{best}} = \frac{\sqrt{3}\pi}{\gamma g T_2}. \qquad [2]$$

The field of view is technically unlimited in stray-field imaging, although the maximum translation of the sample is clearly limited by the probe. In frequency-swept stray-field imaging, we find that the field of view is limited by the sensitivity of the surface coil at depth into the sample.

The arguments leading to the ultimate resolution in Fourier stray-field imaging are just those relating to conventional Fourier magnetic-resonance microscopy, and they have been well rehearsed by a number of authors including Cho (*10*) and Callaghan (*11*). The pixel size is related to the data-acquisition time in the gradient according to

$$\Delta r^{\text{FT}} = \frac{2\pi}{\gamma g T_{\text{acq}}}. \qquad [3]$$

In the limit of optimum resolution, the pixel spacing expressed in frequency units equals the natural linewidth of the sample, $1/\pi T_2$, so that

$$\Delta r^{\text{FT}}_{\text{best}} = \frac{2}{\gamma g T_2}. \qquad [4]$$

It is thus seen that the optimum resolution for the two experiments is very similar. The minimum T_2 for a given resolution is plotted in Fig. 5 for a typical STRAFI gradient strength of 58 T m^{-1}. This plot makes clear why the acetate spacer, which has a short T_2, is not seen in the profiles of Fig. 3.

It might be thought that an increase in T_2 might always yield improved resolution. However, long T_2 values are generally associated with mobile systems to which diffusive broadening in the field gradient applies. This restricts the spin–spin relaxation time to an effective value, T_2^{eff}, which, as has been shown by Callaghan (*12*) amongst others, severely limits the achievable resolution. According to Callaghan,

$$\frac{1}{\pi T_2^{\text{eff}}} \approx 0.6\left(\frac{\gamma^2 g^2 D}{3}\right)^{1/3}, \qquad [5]$$

which, by substitution into Eq. [2] or [4] as appropriate, yields the best achievable resolution for diffusively broadened systems as a function of D, the diffusion coefficient. This result applies for both kinds of STRAFI experiment, since in both cases we are measuring an echo at finite time, 2τ. Figure 5 also includes a plot of D versus best achievable resolution, again evaluated for a gradient strength of 58 T m^{-1}. This analysis shows that for very-high-resolution imaging both techniques are primarily applicable to samples with T_2 values of order 100 μs. If the T_2 is much shorter, then the frequency-swept technique fails because the narrow-band pulse required for high resolution becomes longer than T_2. The Fourier method fails because the signal does not last sufficiently long to record an echo with large enough τ for the required resolution. Neither method is applicable to mobile liquids, since, in the strong gradient, they exhibit a very short, diffusion-limited T_2^{eff}.

By way of comparison, Fig. 5 also shows calculations of achievable resolution based on a gradient strength of 1 T m^{-1}, typical of a conventional MR microscope. It is seen that the stray-field methods offer improved resolution for a given T_2 but are more limited with respect to diffusion, as might be expected. It is worth noting also that diffusion out of the sensitive slice is not likely to be a problem in stray-field imaging. Even for a diffusion coefficient of 2.5×10^{-5} cm^2 s^{-1} (that of water), the diffusion distance $(2Dt)^{1/2}$ is small compared to the best achievable resolution when the corresponding T_2^{eff} is substituted for τ.

No account has been taken in this discussion of the signal-to-noise ratio. Direct comparisons of coil performance are largely irrelevant, because of the less than optimum geometry. The thin-film STRAFI methods and probe system discussed here suffer from loss of sensitivity because of the strength of the gradient and very poor coil sensitivity. Either one of these may be improved individually, but not with the magnet geometry used here. None the less, STRAFI is a very powerful method which allows the imaging of broad-line systems, and this paper demonstrates the extension of these techniques to thin films. Examination of Fig. 3 suggests that the signal-to-noise ratio of the frequency-swept and Fourier STRAFI techniques is comparable and, in the examples considered here, more than adequate. In conventional FT microscopy, it is possible to optimize the signal-to-noise ratio for a given resolution by complementary variation of

the gradient strength and acquisition time. This is clearly not possible with stray-field techniques where the gradient is fixed. However, the ability to visualize short T_2 components, for instance, toward the end of a drying experiment, far outweighs the reduced signal-to-noise ratio consequent on being far from the optimum $1/(\pi T_2)$ experimental bandwidth when T_2 is much longer, for instance, in the early stages of drying.

REFERENCES

1. A. A. Samoilenko, D. Yu. Artemov, and A. L. Sibel'dina, *JETP Lett.* **47,** 348 (1988).
2. H. D. Zeiger, U.S. Patent 5,424,644 (1995).
3. K. L. Perry, P. J. McDonald, E. W. Randall, and K. Zick, *Polymer* **35,** 2744 (1994).
4. A. A. Samoilenko and K. Zick, ''Proceedings of the 26th Congress Ampere'' (A. Anagnostopolous, F. Milia, and A. Simonopolous, Eds.), Athens, p. 40, 1992.
5. D. M. Lane and P. J. McDonald, *Polymer* **38,** 2329 (1997).
6. T. B. Benson and P. J. McDonald, *J. Magn. Reson. A* **112,** 17 (1995).
7. J. B. Miller and A. N. Garroway, U.S. Patent 5,126,674 (1992).
8. P. T. Callaghan, ''Principles of Nuclear Magnetic Resonance Microscopy,'' Clarandon Press, Oxford, 1991.
9. R. R. Ernst, G. Bodenhausen, and A. Wokaun, ''Principles of Nuclear Magnetic Resonance in One and Two Dimensions,'' Chap. 4, Clarandon Press, Oxford, 1987.
10. Z. H. Cho, C. B. Ahn, S. C. Juh, H. K. Lee, R. E. Jacobs, S. Lee, J. H. Yi, and J. M. Jo, *Med. Phys.* **15,** 815 (1988).
11. P. T. Callaghan and C. D. Eccles, *J. Magn. Reson.* **71,** 426 (1987).
12. P. T. Callaghan and C. D. Eccles, *J. Magn. Reson.* **78,** 1 (1988).